Atmos. Chem. Phys. Discuss., 11, 21769–21787, 2011
www.atmos-chem-phys-discuss.net/11/21769/2011/
doi:10.5194/acpd-11-21769-2011
© Author(s) 2011. CC Attribution 3.0 License.

Atmospheric Chemistry and Physics Discussions

This discussion paper is/has been under review for the journal Atmospheric Chemistry and Physics (ACP). Please refer to the corresponding final paper in ACP if available.

Variation of upper tropospheric clouds and water vapor over the Indian ocean

R. L. Bhawar[1], **J. H. Jiang**[1], **and H. Su**[1]

[1]Jet Propulsion Laboratory, California Institute of Technology, Pasadena, CA 91109, USA

Received: 8 July 2011 – Accepted: 28 July 2011 – Published: 2 August 2011

Correspondence to: R. L. Bhawar (rohinibhawar@gmail.com)

Published by Copernicus Publications on behalf of the European Geosciences Union.

Abstract

The upper tropospheric (UT) ice water content (IWC) and water vapor (H_2O) observed by the Microwave Limb Sounder (MLS) show dominant dipole mode variability over the Indian Ocean. This is characterized by the oscillating differences between the Western and Eastern Indian Ocean (WIO and EIO) with greater amplitude in JJA and SON than in other seasons. We denote $\delta X = X\_WIO - X\_EIO$, with X being H_2O and IWC at three UT levels (215 hPa, 147 hPa and 100 hPa) as well as sea surface temperature (SST), following the definition for previously identified Indian Ocean Dipole (IOD) variability. We found a strong positive correlation of δIWC at three UT levels with δSST, and a relatively weak positive correlation of δIWC with Nino 3.4 SST, suggesting that the UT clouds over the Indian Ocean are largely controlled by local thermally-driven circulation while teleconnection to ENSO plays a secondary role. The change per degree of δSST for δIWC in SON is 5.5 mg m^{-3} C^{-1} at 215 hPa, 1.6 mg m^{-3} C^{-1} at 147 hPa and 0.13 mg m^{-3} C^{-1} at 100 hPa (the 7-yr mean δIWC is -4.7 mg m^{-3}, -1.6 mg m^{-3} and -0.13 mg m^{-3} at 215 hPa, 147 hPa and 100 hPa respectively). For δH_2O, the per degree δSST change of 41.2 ppmv C^{-1} corresponds to a strong increase at 215 hPa and a decrease of -0.23 ppmv C^{-1} (-0.18 ppmv C^{-1}) at 100 hPa (147 hPa), respectively. The Nino 3.4 SST has a relatively weak positive (negative) correlation with δH_2O at 215 hPa (100 hPa). The increase of δH_2O at 215 hPa with increasing δSST is associated with the sharper contrast in convective intensity while the decrease of δH_2O at 100 hPa with increasing δSST is a signature of the "convective cold top" and temperature control of 100 hPa H_2O. For H_2O, the 147 hPa marks a transition from the convection-controlled 215 hPa to the temperature-controlled 100 hPa.

1 Introduction

The interannual variability over the Indian Ocean is influenced by both large-scale dynamics and internal Indian Ocean dynamics. In recent years, there have been a

ACPD
11, 21769–21787, 2011

number of studies on the interannual variability in the tropical Indian Ocean (e.g., Perigaud and Delecluse, 1993; Masumoto and Meyers, 1998), with increasing focus on Indian Ocean Dipole events (Behera et al., 1999; Vinayachandran et al., 1999; Webster et al., 1999; Saji et al., 1999). The thermal structure of the equatorial Indian Ocean is characterized by warmer (cooler) sea surface temperature (SST) in the east (west) as a consequence of the upwelling along the western boundary and strong eastward equatorial jets that transport warm upper layer water to the east (Vinaychandran et al., 2007). Using observational data over the past 40 yr, a pattern of internal variability with anomalously low SST off Sumatra in the Eastern Indian Ocean (EIO) and anomalously high SST in the western Indian Ocean (WIO) was identified. This SST anomaly pattern accompanied by similar wind and precipitation anomalies was reported as the Indian Ocean Dipole (IOD) (Saji et al., 1999; Webster et al., 1999). A positive IOD event refers to negative SST anomalies in the EIO and positive SST anomalies in the WIO. This oscillatory mode of coupled ocean–atmosphere variability causes climatic extremes such as droughts in East Asia and Australia and floods in parts of India and East Africa during austral winter and spring (Saji et al., 1999; Meyers et al., 2007).

In this paper we study the variations of upper tropospheric (UT) ice water content (IWC) and water vapor (H_2O) observed by Aura Microwave Limb Sounder (MLS) in association with SST over the Indian Ocean with a focus on the variability related to the IOD. UT clouds have important radiative effects on the Earth-atmosphere system (Liou., 1986). They are closely related to UT humidity, which is the dominant contributor to the greenhouse effect (e.g., Lindzen, 1990; Sun and Lindzen, 1993; Soden and Fu, 1995; Su et al., 2006, 2008 and 2009). One of the greatest challenges in climate model simulations and climate change predictions is to accurately represent these UT clouds, their radiative effects and associated climate feedbacks (Cess et al., 1996; Stephens, 2005). Aura MLS provides unique UT observations of IWC and H_2O at different vertical levels from 260 hPa and above. Correlations of these UT observations with SST provide a perspective to understand the dynamical processes involving deep convection and ocean-atmosphere coupling. We also perform a quantitative analysis

ACPD
11, 21769–21787, 2011

of these relationships in order to determine potential of water vapor and cloud climate feedbacks.

2 Data sets

MLS Level 2, IWC, H_2O and temperature measurements from September 2004 to December 2010 (7-yr) and National Center for Environmental Prediction (NCEP) SST and air temperature data for the same period are used for this study. MLS measures ~3500 vertical profiles per day along a sun-synchronous sub-orbital track with equatorial crossings at 01:40 p.m. and 01:40 a.m. local solar times. MLS data version 2.2 provides H_2O and IWC above 215 hPa with a vertical resolution about ~3–4 km (Livesey et al., 2007, Jiang et al., 2010). The MLS H_2O single measurement precision varies from ~25 % at 316 hPa to ~10 % at 100 hPa, with an expected accuracy of ~10 %. For IWC the precision ranges from ~0.6–1.3 mg m^{-3} at 215 hPa, 0.2 mg m^{-3} at 147 hPa and 0.07 mg m^{-3} at 100 hPa (Wu et al., 2008). Estimated measurement accuracy is a factor of two for IWC (Jiang et al., 2010). MLS temperature at 215 hPa has a cold bias of 1–2 K over the cloudy regions (Schwartz et al., 2008). The MLS data have horizontal resolutions of ~200–300 km along-track and ~7 km across-track (Wu et al., 2008).

The SST anomalies were computed relative to the mean over the MLS measurement period from 2004–2010. The region considered in the study is the Indian Ocean region 50° E to 110° E and 10° S to 10° N. Monthly and seasonal data have been analyzed for UT IWC and H_2O at 215 hPa, 147 hPa, and 100 hPa pressure levels.

3 Results and discussion

3.1 Seasonal maps

Figure 1a and b show the seasonal anomaly maps for June-August (JJA) and September-November (SON) for SST, H_2O and IWC at 215 hPa during the years

ACPD
11, 21769–21787, 2011

2004–2010. The climatological means are constructed for each season from 2004 to 2010. Since MLS observations started in August 2004, JJA maps start from year 2005. The boxes marked in the SST maps indicate the two regions WIO (50° E–70° E and 10° S–10° N) and EIO: (90° E–110° E and 10° S–0° S) between which the dipole pattern oscillates. In both JJA and SON seasons, positive SST anomalies in the WIO box tend to be associated with positive H_2O and IWC anomalies, accompanied by negative SST, H_2O and IWC anomalies in the EIO box at 215 hPa. During SON in 2006 we observe strong positive H_2O and IWC anomalies in WIO and negative anomalies in EIO, in phase with the SST anomalies, approximately resembling a positive IOD pattern. On the contrary, a strong negative IOD pattern is observed in the year 2010 with positive anomaly for IWC and H_2O in EIO and negative anomaly in WIO. We also found the signatures of this dipole pattern at 147 hPa and 100 hPa. There is no clear periodic oscillation of this dipole pattern during MAM and DJF.

3.2 EOF Analysis

We performed empirical orthogonal function (EOF) analysis on the monthly MLS IWC anomalies over the Indian Ocean domain for June–November for period of 2004–2010. Using this method, the bulk of the variance of a data set can be described by a few orthogonal modes, so that the dominant modes of variability can be easily identified (Lee et al., 2003). Figure 2 shows the first three EOF modes for these 39 monthly samples. The leading EOF mode (mode 1) explains 25 % variance and shows a dipole pattern while the 2nd and 3rd modes explain 12 % and 8 % variance respectively. This confirms the dominant variability in the Indian Ocean is indeed a dipole pattern. We also carried out the EOF analysis using all the monthly data (76 months) from September 2004 to December 2010 (not shown). The dipole mode emerges as a dominant mode with 16 % variance and the 2nd and 3rd modes explain 11 % and 7 % variance, respectively.

ACPD
11, 21769–21787, 2011

3.3 Time Series of SST and IWC for the Dipole Mode

The intensity of the IOD is usually represented by the anomalous SST difference between the WIO and the EIO. This difference is termed the Dipole Mode Index (DMI) (Saji et al., 1999). Figure 3a shows a time series of DMI index calculated over the period of September 2004 to December 2010 with positive DMI corresponding to positive IOD events. The dashed lines at ±0.5 °C distinguish between the weak (DMI ≤ 0.5^{o}C) and strong IOD (DMI ≥0.5 °C) events. From September 2004 to December 2010, there are 3 strong positive IOD events (during 2006, 2007 and 2008) and 3 strong negative IOD events (2 during 2005 and one in 2010). In the year 2006 we see a strong peak of more than 1.0 °C in DMI during October; in 2007 DMI peaked in September and in 2008 it peaked during July and diminished in October. These three consecutive positive IODs are of rare occurrence (Cai et al., 2009). The 3 strong negative dipole modes peaked in March 2005, September 2005 and October 2010.

Figure 3b shows the monthly time series of IWC anomalies at 215 hPa from September 2004 to December 2010 for the WIO and EIO separately. An anti-correlation is shown between the WIO and EIO IWCs. The three strong positive IOD events stand out as the red troughs over the EIO region and black ridges over the WIO region, while the 3 negative IOD events show approximately opposite responses in the EIO and WIO.

3.4 IWC and H_2O Relation with SST

Given that the dipole mode dominates the interannual variability; we define δX as the difference between WIO and EIO where X is H_2O, IWC or temperature (T) at three UT levels, or SST. The relations of δIWC, δH_2O and δT with δSST are examined, along with their relations with Nino3.4 SST anomalies in order to distinguish the local Indian Ocean forcing from the remote Pacific forcing associated with the El Nino-Southern Oscillation (ENSO).

The top panels of Fig. 4 shows scatter plots of δIWC, δH_2O and δT at three levels versus δSST for SON. The lower panels show the scatter plots of δIWC, δH_2O and

ACPD
11, 21769–21787, 2011

δT versus Nino 3.4 SST for SON. Each dot corresponds to a SON average for a certain year (2004–2010). From the scatter plots of δIWC versus δSST we find a strong positive correlation of more than 0.95 (statistical significance level above 99 %) for all 3 levels at 215 hPa, 147 hPa and 100 hPa. This indicates that as δSST increases, the difference in deep convection between WIO and EIO increases, leading to positive δIWC. All the points are clustered along the linear fit. The rate of increase in δIWC is 5.5 mg m^{-3} C^{-1} at 215 hPa, 1.6 mg m^{-3} C^{-1} at 147 hPa and 0.13 mg m^{-3} C^{-1} at 100 hPa (the 7-yr mean δIWC is −4.7 mg m^{-3}, −1.6 mg m^{-3} and −0.13 mg m^{-3} at 215 hPa, 147 hPa and 100 hPa, respectively). Su et al. (2008) suggest an increase of 15 % K^{-1} at 215 hPa, 34 % K^{-1} at 147 hPa and 60 % K^{-1} at 100 hPa for 15° S–15° N tropical mean IWC during the period from 8 August 2004 to 30 September 2006.

For δH_2O versus δSST, we observe a positive correlation of about 0.93 at 215 hPa and a negative correlation of −0.3 and −0.5 at 147 hPa and 100 hPa respectively. The slope of δH_2O versus δSST is 41.2 ppmv C^{-1} at 215 hPa, −0.18 ppmv C^{-1} at 147 hPa and −0.23 ppmv C^{-1} at 100 hPa (with 7-yr mean δH_2O values of −56.1 ppmv, −0.63 ppmv and 0.52 ppmv at three levels). We also plotted the MLS temperature in order to understand variations in UT water vapor. The strong increase in δH_2O at 215 hPa with δSST is related to the greater convection contrast between WIO and EIO due to the SST difference. The presence of cold bias in the 215 hPa MLS temperature over the cloudy regions yields a negative δH_2O-δT relation. Hence, we looked at the NCEP air temperature at 200 hPa. We observe an increase in 215 hPa δH_2O with δSST, in phase with the increase in δIWC, and an increase of δT from NCEP, suggesting that convective transport is predominant in determining the H_2O changes at 215 hPa.

On the other hand, δH_2O at 147 and 100 hPa appears to be negatively correlated with δSST but in phase with δT at the same level. This is consistent with the "convective cold top" observation and theory elaborated upon by Holloway and Neelin (2007). Above enhanced convection, temperature is usually colder than normal. Hence, positive δSST would cause negative δT in the tropical tropopause layer (TTL). In this layer,

ACPD
11, 21769–21787, 2011

especially at 100 hPa, change of water vapor is primarily governed by change of temperature (Jiang et al., 2010; Liu et al., 2007). The level of 147 hPa is a transition level between the convection-dominated 215 hPa to temperature-controlled 100 hPa, thus δH_2O at this level has a weak correlation with δSST. The change in δH_2O at 100 hPa with δSST is $-0.23\,\mathrm{ppmv\,C^{-1}}$ in comparison to $-0.18\,\mathrm{ppmv\,C^{-1}}$ at 147 hPa.

From the correlations of δIWC and δH_2O with δSST, we can clearly see that local Indian Ocean SST strongly governs the UT clouds and water vapor variability via the changes in deep convection intensity. However, previous studies indicate that precipitation (convection) in the Indian Ocean is also impacted by ENSO (e.g., Su et al., 2001, Zhong et al., 2005) through an "atmospheric bridge" (Alexander et al., 1992). The bottom panels of Fig. 4 show the scatter plots of δIWC, δH_2O and δT at three UT levels vs Nino 3.4 SST anomalies for SON. A positive correlation of about 0.4 is found between δIWC and Nino 3.4 SST. The rate of increase of δIWC is $1.9\,\mathrm{mg\,m^{-3}\,C^{-1}}$ at 215 hPa, $0.48\,\mathrm{mg\,m^{-3}\,C^{-1}}$ at 147 hPa and $0.03\,\mathrm{mg\,m^{-3}\,C^{-1}}$ at 100 hPa. For δH_2O we observe a positive slope of $7.8\,\mathrm{ppmv\,C^{-1}}$ at 215 hPa, and a negative slope of -0.11 ppmv C and $-0.16\,\mathrm{ppmv\,C^{-1}}$ at 147 hPa and 100 hPa with Nino 3.4 SST, respectively. Thus, there appears to be a positive correlation between the dipole mode and ENSO, though the ENSO influence on the UT water vapor and cloud dipole modes is significantly weaker than the local SST dipole effect. We also observe a similar relationship during JJA (not shown) to that in SON. We found a negative correlation of δH_2O with Nino 3.4 SST over the EIO region and a positive correlation over the WIO region. We speculate that this negative correlation over EIO is due to the teleconnection from the Pacific over the Indian Ocean. The resultant positive correlation of δH_2O over WIO with Nino 3.4 SST might be due to the coincidental increased convection in the presence of local SST anomalies, as δSST and Nino 3.4 SST have a positive correlation of 0.4.

ACPD
11, 21769–21787, 2011

4 Summary

Based on the EOF analysis of 7-yr of MLS IWC observations, a dipole mode oscillating between WIO and EIO is found to be the dominant mode in the UT on an interannual time scale over the Indian Ocean for June-November. The relationships of the UT IWC and H_2O dipoles with the Indian Ocean SST dipole anomaly and with the Nino3.4 SST anomaly over the Pacific Ocean are examined. We found that there are strong positive correlations between local WIO and EIO SST difference (δSST) and the UT dipole parameters (δIWC, δH_2O and δT). Our study estimates an increase in δIWC due to local δSST changes, as well as Nino 3.4 SST anomalies. For δH_2O we found a definite increase at 215 hPa strongly related to local SST dipole anomaly. At 100 hPa, a negative correlation of −0.5 is observed between δH_2O and δSST with a slope of $-0.23\,\mathrm{ppmv\,C^{-1}}$. A similar negative correlation of −0.5 was found between δH_2O and Nino 3.4 SST at 100 hPa with a slope of −0.16 ppmv C. The 147 hPa level appears to be a transition between the 215 and 100 hPa, with correlations in-between the two levels and in-phase with those at 100 hPa.

Summarizing the correlations we have examined, Fig. 5 schematically illustrates the physical processes that govern the interannual variabilities of UT clouds and water vapor observed by MLS. The primary driver for the UT IWC and H_2O dipole modes is the local Indian SST dipole, which induces oppositely phased convective anomalies in the WIO and EIO, causing the dipole patterns in UT IWC and H_2O at 215 hPa. The IWC changes are vertically coherent but H_2O switches sign in the TTL. Above convection, cold temperature anomalies are produced, leading to negative H_2O anomalies, opposite to the positive H_2O anomalies at 215 hPa.

Apart from the local SST influence, the UT over the Indian Ocean is also influenced by the SST anomalies in the Eastern/Central Pacific Ocean associated with ENSO. During the warm phase of El Nino, anomalously strong convection over the Pacific would cause abnormal subsidence over the Indian Ocean through an “atmospheric bridge”. It appears to us that the forced subsidence over the EIO (in addition to the

ACPD
11, 21769–21787, 2011

anomalous subsidence induced by local SST anomalies) strengthens the dipole pattern induced by the local Indian Ocean SST dipole anomalies. However, the influence of this teleconnection on the UT dipole pattern is weaker than the local SST dipole forcing. We suppose there may be an influence on the EIO region through the atmospheric teleconnection from the Pacific. The potential influence of ENSO on the WIO and EIO requires further study.

Acknowledgements. The authors acknowledge the National Centers for Environmental Prediction (NCEP) for the surface parameters. The work was carried out at the Jet Propulsion Laboratory, California Institute of Technology, under contract with NASA. We also thank Jennifer Small for helpful comment and reviewing early version of this manuscript.

References

Abram, N. J., Gagan, M. K., McCulloch, M. T., Chappell, J., and Hantoro W. S.: Coral Reef Death During the 1997 Indian Ocean Dipole Linked to Indonesian Wildfires, Science, 952–955, doi:10.1126/science.1083841, 2003.

Alexander, M. A.: Midlatitude atmosphere-ocean interaction during El Nino, part I, The North Pacific Ocean, J. Clim., 5, 944–958, 1992.

Ashok, K. and Saji, N. H.: On impacts of ENSO and Indian Ocean Dipole events on the sub-regional Indian summer monsoon rainfall, Nat. Hazards, 42(2), 273–285, doi:10.1007/s11069-006-9091-0., 2007.

Behera, S. K., Krishnan, R., and Yamagata, T.: Unusual ocean-atmosphere conditions in the tropical Indian Ocean during 1994, Geophys. Res. Lett., 26, 3001–3004, 1999.

Birkett, C., Murtugudde, R., and Allan, R.: Indian Ocean climate event brings floods to East Africa's lakes and the Sudd Marsh, Geophys. Res. Lett., 26, 1031–1034, 1999.

Cai, W., Pan, A., Roemmich, D., Cowan, T., and Guo, X.: Argo profiles a rare occurrence of three consecutive positive Indian Ocean Dipole events, 2006–2008, Geophys. Res. Lett., 36, L08701, doi:10.1029/2008GL037038, 2009.

Cess, R. D., Zhang, M. H., Ingram, W. J., Potter, G. L., Alekseev, V., Barker, H. W., Cohen-Solal, E., Colman, R. A., Dazlich, D. A., Del Genio, A. D., Dix, M. R., Dymnikov, V., Esch, M., Fowler, L. D., Fraser, J. R., Galin, V., Gates, W. L., Hack, J. J.,Kiehl, J. T., Le Treut, H., Lo, K.

ACPD

11, 21769–21787, 2011

K.-W., McAvaney, B. J., Meleshko, V. P., Morcrette, J.-J., Randall, D. A., Roeckner, E., Royer, J.-F., Schlesinger, M. E., Sporyshev, P. V., Timbal, B., Volodin, E. M., Taylor, K. E., Wang, W., and Wetherald, R. T.: Cloud feedback in atmospheric general circulation models: An update, J. Geophys. Res., 101(D8), 12791–12794, 1996.

Holloway, C. E. and Neelin, J. D.: The convective cold top and quasi equilibrium, J. Atmos. Sci., 64, 1467–1487, 2007.

Jiang, J. H., Su, H., Pawson, S., Liu, H. C., Read, W., Waters, J. W., Santee, M., Wu, D. L., Schwartz, M., Livesey, N., Lambert, A., Fuller, R., and Lee, J. N.: Five-year (2004-2009) Observations of Upper Tropospheric Water Vapor and Cloud Ice from MLS and Comparisons with GEOS-5 analyses, J. Geophys. Res., 115, D15103, doi:10.1029/2009JD013256, 2010.

Lee, M. A., Yeah, C. D., Cheng, C. H., Chan, J. W., and Lee, K. T.: Empirical orthogonal function analysis of AVHRR sea surface temperature patterns in Taiwan strait, J. Mar. Sci. Technol., 11(1), 1–7, 2003.

Lin, J.-L., Kiladis, G. N., Mapes, B. E., Weickmann, K. M., Sperber, K. R., Lin, W., Wheeler, M. C., Schubert, S. D., Del Genio, A., Donner, L. J., Emori, S., Gueremy, J.-F., Hourdin, F., Rasch, P. J., Roeckner, E., and Scinocca, J. F.: Tropical intraseasonal variability in 14 IPCC AR4 climate models. Part I: Convective signals, J. Climate, 19, 2665–2690, doi:10.1175/JCLI3735.1, 2006.

Lindzen R. S.: Some coolness concerning global warming, Bull. Am, Meteorol. Soc., *71*, 288–299, (1990).

Lindzen, R., Chou, M., and Hou, A.: Does the Earth Have an Adaptive Infrared Iris?, Bull. Amer. Meteor. Soc., 82, 417–432, 2001.

Liou, K. N.: Influence of cirrus clouds on weather and climate processes: a global perspective, Mon. Weather Rev, 114, 1167–1199, 1986.

Livesey, N. J., Read, W. G., Lambert, A., Cofield, R. E., Cuddy, D. T., Froidevaux, L., Fuller, R. A., Jarnot, R. F., Jiang, J. H., Jiang, Y. B., Knosp, B. W., Kovalenko, L. J. , Pickett, H. M., Pumphrey, H. C., Santee, M. L., Schwartz, M. J., Stek, P. C., Wagner, P. A., Waters, J. W., and Wu, D. L.: EOS MLS Version 2.2 Level 2 data quality and description document, JPL technical report, D-33509., 2007.

Liu, C., Zipser, E., Garrett, T., Jiang, J., and Su, H.: How do the water vapor and carbon monoxide "tape recorder" start near the tropical tropopause?, Geophys. Res. Lett., 34, L09804, doi:10.1029/2006GL029234, 2007.

Luo, Z. J., Kley, D., Johnson, R. H., Liu, G. Y., Nawrath, S., and Smit, H. G. J.: Influence of sea

ACPD
11, 21769–21787, 2011

surface temperature on humidity and temperature in the outflow of tropical deep convection, J. Climate, in review, 2011.
Masumoto, Y. and Meyers, G.: Forced Rossby waves in the southern tropical Indian Ocean, J. Geophys. Res., 103, 27589–27602, 1998.
Meyers, G., McIntosh, P., Pigot, L., and Pook, M.: The years of El Niño, La Niña, and interactions with the tropical Indian Ocean, J. Climate, 20, 2872–2880, 2007.
Perigaud, C. and Delecluse, P.: Interannual Sea Level Variations in the Tropical Indian Ocean from Geosat and Shallow Water Simulations, J. Phys. Oceanogr., 23, 1916–1934, 1993.
Webster, P. J., Moore, A. M., Loschnigg, J. P., and Leben, R. R.: Coupled ocean-atmosphere dynamics in the Indian Ocean during 1997–98, Nature, 401(6751), 356–360, 1999.
Saji, N. H., Goswami, B. N., Vinayachandran, P. N., and Yamagata, T.: A dipole mode in the tropical Indian Ocean, Nature, 401(6751), 360–363, 1999.
Schwartz, M. J., Lambert, A., Manney, G. L., Read, W. G., Livesey, N. J., Froidevaux, L., Ao, C. O., Bernath, P. F., Boone, C. D., Cofield, R. E., Daffer, W. H., Drouin, B. J., Fetzer, E. J., Fuller, R. A., Jarnot, R. F., Jiang, J. H., Jiang, Y. B., Knosp, B. W., Kruger, K., Li, J.-L. F., Mlynczak, M. G., Pawson, S., Russell, J. M., Santee, M. L., Snyder, W. V., Stek, P. C., Thurstans, R. P., Tompkins, A. M., Wagner, P. A., Walker, K. A., Waters, J. W., and Wu, D. L.: Validation of the Aura Microwave Limb Sounder Temperature and Geopotential Height Measurements, J. Geophys. Res., 113, D15S11, doi:10.1029/2007JD008783, 2008.
Soden, B. J. and Fu, R.: A satellite analysis of deep convection, upper-tropospheric humidity, and the greenhouse effect, J. Climate, 8, 2333–2351, 1995.
Stephens, G. L.: Cloud feedbacks in the climate system: A critical review, J. Clim., 18, 237–273, 2005.
Su, H., Read, W. G., Jiang, J. H., Waters, J. W., Wu, D. L., and Fetzer, E. J.: Enhanced positive water vapor feedback associated with tropical deep convection: New evidence from Aura MLS, Geophys. Res. Lett., 33, L05709, doi:10.1029/2005GL025505, 2006.
Su, H., Jiang, J. H., Gu, Y., Neelin, J. D., Kahn, B. H., Feldman, D., Yung, Y. L., Waters, J. W., Livesey, N. J., Santee, M. L., and Read, W. G.: Variations of tropical upper tropospheric clouds with sea surface temperature and implications for radiative effects, J. Geophys. Res., 113, D10211, doi:10.1029/2007JD009624, 2008.
Su, H., Jiang, J. H., Stephens, G. L., Vane, D. G., and Livesey, N. J.: Radiative effects of upper tropospheric clouds observed by Aura MLS and CloudSat, Geophys. Res. Lett., 36, L09815, doi:10.1029/2009GL037173, 2009.

ACPD
11, 21769–21787, 2011

Su, H., Neelin, J. D., and Chou, C.: "Tropical teleconnection and local response to SST anomalies during the 1997–1998 El Nino", J. Geophys. Res., 106, 20025–20043, 2001.
Sun, D.-Z. and Lindzen, R. S.: Distribution of tropical tropospheric water vapor, J. Atmos. Sci., 50, 1643–1660, 1993.
Vinaychandran, P. N., Saji, N. H., and Yamagata, T.: Response of the Equatorial Indian Ocean to an unusual wind event during 1994, Geophys. Res. Lett., 26, 1613–1616, 1999.
Vinayachandran, P. N., Kurian, J., and Neema, C. P.:, Indian Ocean response to anomalous conditions during 2006, Geophys. Res. Lett., 34, L15602, doi:10.1029/2007/GL030194, 2007.
Wu, D. L., Jiang, J. H., Read, W. G., Austin, R. T., Davis, C. P., Lambert, A. Stephens, G. L., Vane, D. G., and Waters, J. W.: Validation of the Aura MLS cloud ice water content measurements, J. Geophys. Res., 113, D15S10, doi:10.1029/2007JD008931, 2008.
Zhong, A., Hendon, H. H., and Alves, O.: Indian Ocean variability and its association with ENSO in a Global coupled model, J. Climate, 18, 3634–3649, 2005.

ACPD
11, 21769–21787, 2011

Table 1. Shows the slopes and correlation coefficients for IWC and H_2O at 3 pressure levels 215 hPa, 147 hPa and 100 hPa for WIO-EIO box.

Sep–Nov	Ice water Content ($mg\,m^3\,C^{-1}$)		Water Vapour ($ppmv\,C^{-1}$)	
West-East Indian Ocean box	5.52	0.96	41.28	0.93
215 hPa	1.67	0.97	−0.185	−0.33
147 hPa	0.138	0.96	−0.23	−0.51
100 hPa				
Sep–Nov Nino 3.4	**Ice water Content ($mg\,m^3\,C^{-1}$)**		**Water Vapour ($ppmv\,C^{-1}$)**	
West-East Indian Ocean box				
215 hPa	1.89	0.55	7.81	0.29
147 hPa	0.48	0.46	−0.112	−0.34
100 hPa	0.03	0.45	−0.161	−0.58

ACPD
11, 21769–21787, 2011

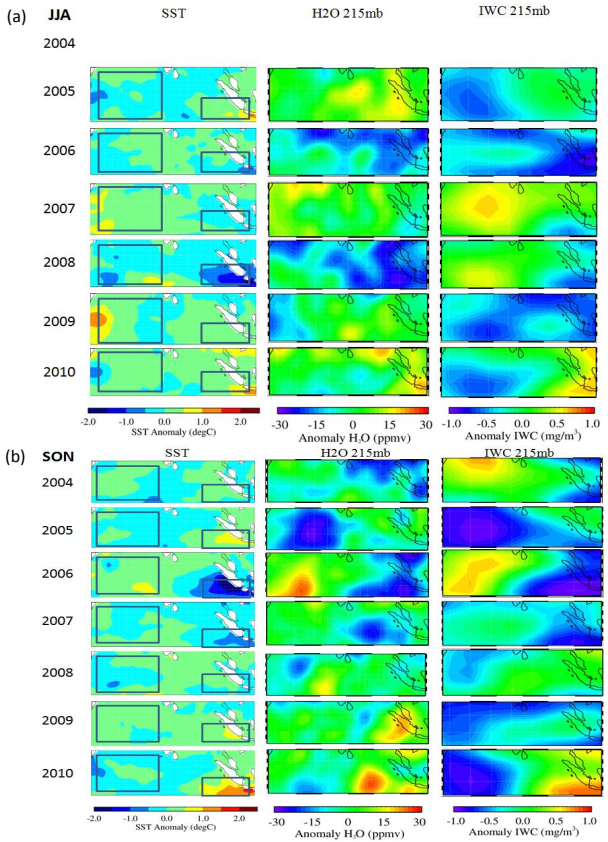

Fig. 1. **(a)** SST, H_2O and IWC anomaly at 215 hPa for June–August **(b)** SST, H_2O and IWC anomaly for September–November. The boxes indicated in the first column are the WIO (50° E–70° E and 10° S–10° N) and EIO (90° E–110° E and 10° S–0° S) regions.

ACPD
11, 21769–21787, 2011

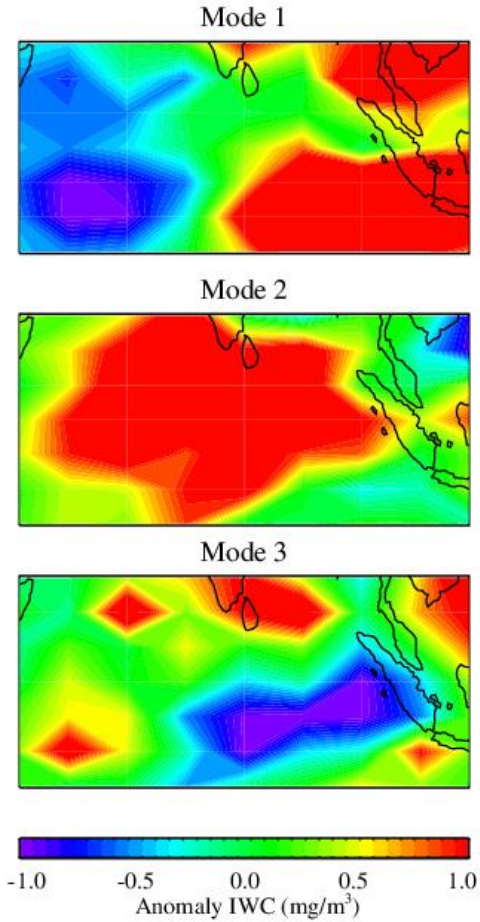

Fig. 2. The three EOF modes in the Indian Ocean domain for IWC at 215 hPa.

ACPD
11, 21769–21787, 2011

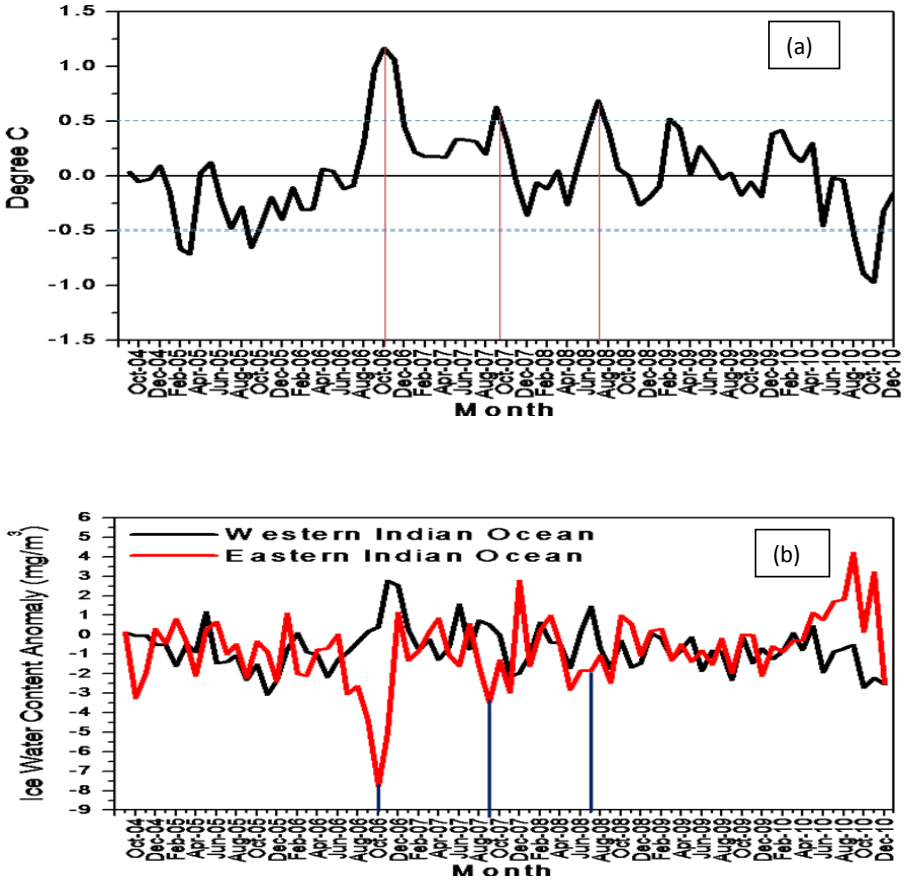

Fig. 3. Top panel represents the Monthly Dipole Mode Index (DMI) for the period September 2004–December 2010 and bottom panel represents Time series of IWC anomaly at 215 hPa over the Western Indian Ocean box and the Eastern Indian Ocean box.

ACPD
11, 21769–21787, 2011

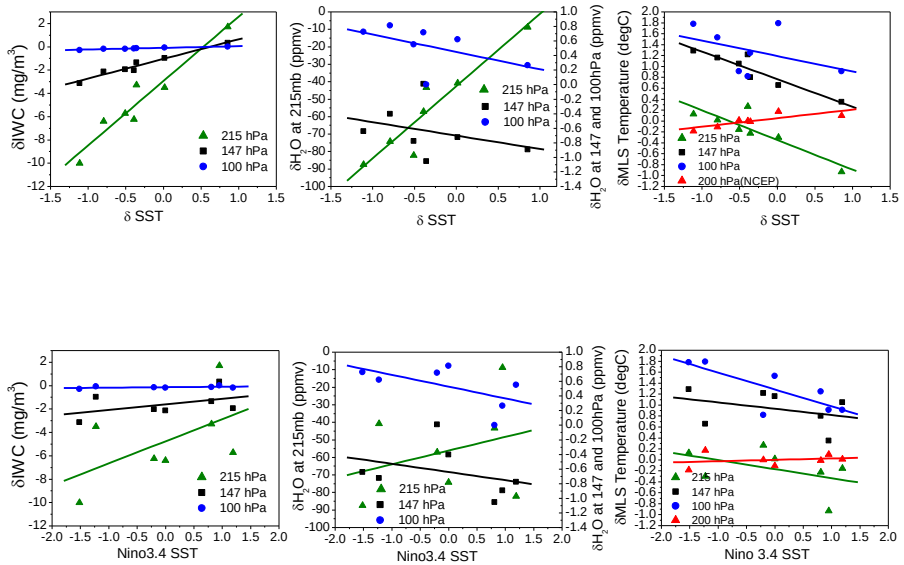

Fig. 4. Top panel scatter plots for δIWC, δH_2O and δtemperature vs. δSST for September–November. Bottom panel scatter plots for δIWC, δH_2O and δ temperature vs Nino 3.4 SST for September–November.

ACPD
11, 21769–21787, 2011

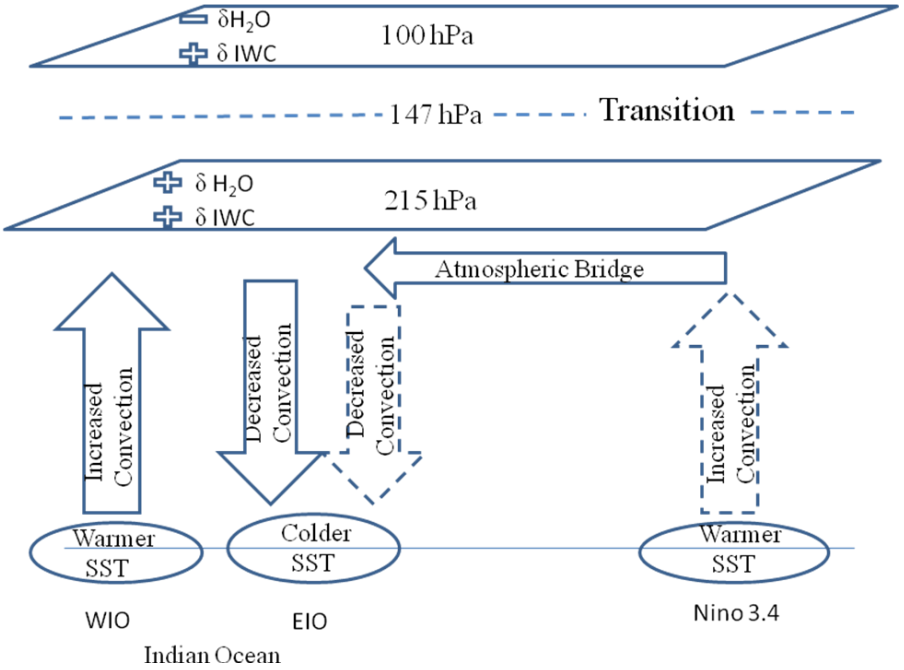

Fig. 5. Schematic diagram showing the local and large-scale effects over Indian Ocean domain. (δ refers to WIO–EIO).

ACPD
11, 21769–21787, 2011